Chemical Engineering Science 175 (2018) 40–55

Contents lists available at ScienceDirect

Chemical Engineering Science

journal homepage: www.elsevier.com/locate/ces

Mathematical modelling of water absorption and evaporation in a pharmaceutical tablet during film coating

Charalampos Christodoulou [a], Eva Sorensen [a], Salvador García-Muñoz [b], Luca Mazzei [a,*]

[a] Department of Chemical Engineering, University College London, Torrington Place, London WC1E 7JE, UK
[b] Eli Lilly and Company, Lilly Research Laboratories, Indianapolis, IN 46285, USA

HIGHLIGHTS

- We study spreading, absorption and evaporation after droplet impingement on a tablet.
- We divided the droplet behaviour into three phases of different dynamics.
- Our model simulates droplet impact, water absorption and evaporation on a tablet.
- We validated the model with experimental data from the literature.

ARTICLE INFO

Article history:
Received 31 May 2017
Received in revised form 18 August 2017
Accepted 12 September 2017
Available online 15 September 2017

Keywords:
Pharmaceutical coating
Droplet impact
Absorption
Evaporation
Porous tablets
Mathematical modelling

ABSTRACT

It is well understood that during the pharmaceutical aqueous film coating process the amount of liquid water that interacts with the porous tablet core can affect the quality of the final product. Therefore, understanding and simulating the mechanisms of water droplet spreading, absorption and evaporation is crucial for controlling the process and optimising the shelf-life of the tablets. The purpose of the work presented in this paper is to define and describe the spreading, absorption and evaporation phenomena after droplet impingement on a tablet. We divided the droplet behaviour into three phases of different dynamics and duration: the kinematic, capillary and evaporation phases. To model the kinematic phase, we combined and modified 1-D spreading models from the literature which solve the kinetic energy balance equation for the first milliseconds of spreading. For the capillary phase, we simplified and solved the continuity and Navier-Stokes equations using the lubrication approximation theory. Finally, for the evaporation phase, we adopted a modelling approach for the second drying stage of slurry droplets inside a spray dryer. During this stage, one can no longer describe the droplet as a liquid system containing solids, having to regard it as a wet particle with a dry crust and a wet core. In our work, we represented in a novel way the crust as the dry surface of the tablet and the wet core as the wetted area inside the porous matrix. We implemented the mathematical model presented in this work in gPROMS, employing the Modelbuilder platform. Our numerical results (droplet height and spreading, wetting, evaporation front profiles) are in good agreement with recent experimental data that we found in the literature.

1. Introduction

Aqueous film coating is a crucial step in the manufacture of solid-dosage drugs in the pharmaceutical industry. It is well understood that the shelf life of pharmaceutical tablets depends on the amount of humidity to which they are exposed during the coating process, the handling of the intermediate coated product and the packaging (Amidon et al., 1999). Understanding and being able to predict the mechanisms of water absorption onto and into tablets, is therefore important to avoid accelerating the degradation mechanisms caused by high water content.

During tablet coating a liquid solution is sprayed onto the solid tablet surface. Several researchers have investigated the impact of a droplet on an impermeable substrate, mainly for inkjet printing applications. Park et al. (2003) developed a mathematical model to estimate the maximum spreading factor at low impact velocity. They defined the spreading factor as the ratio of the cyclical wetted area diameter at time t to the initial droplet diameter of the spherical droplet just before impact. Attane et al. (2007) developed an analytical 1-D model based upon the energy equation. By assuming the shape of a droplet (either spherical cap or cylindrical), Attane

* Corresponding author.
E-mail address: l.mazzei@ucl.ac.uk (L. Mazzei).

https://doi.org/10.1016/j.ces.2017.09.021
0009-2509/

Nomenclature

A	surface area (m^2)
c_p	specific heat ($J\ kg^{-1}\ K^{-1}$)
C_v	vapour concentration ($mol\ m^{-3}$)
D	droplet diameter (m)
$\mathcal{D}$	diffusion coefficient ($m^2\ s^{-1}$)
d_p	pore diameter (m)
E_g	gravitational energy (J)
E_k	kinetic energy (J)
E_p	potential energy (J)
E_s	surface energy (J)
h	droplet height profile (m)
h_D	mass transfer coefficient ($m\ s^{-1}$)
h_m	droplet mass centre height (m)
H_p	evaporation front depth (m)
h_p	wetting front depth profile (m)
h_s	precursor film height (m)
h_{ep}	wetted region height (m)
h_{fg}	specific heat of evaporation ($J\ kg^{-1}$)
h_{heat}	heat transfer coefficient ($W\ m^{-2}\ K^{-1}$)
J	evaporation velocity ($m\ s^{-1}$)
k	thermal conductivity ($W\ m^{-1}\ K^{-1}$)
K_Λ	dissipation fitted parameter (dimensionless)
k_p	porous media permeability (m^2)
$\dot{m}_v$	vapour mass flux ($kg\ s^{-1}\ m^{-2}$)
$M_{w,l}$	molecular weight ($kg\ mol^{-1}$)
n	disjoining pressure parameter (dimensionless)
Nu	Nusselt number (dimensionless)
Oh	Ohnesorge number (dimensionless)
p	pressure (Pa)
Pr	Prandtl number (dimensionless)
R_t	wetted area radius (m)
Re	Reynolds number (dimensionless)
RH	relative humidity (dimensionless)
S_{ep}	diameter of the evaporation surface (m)
Sc	Schmidt number (dimensionless)
Sh	Sherwood number (dimensionless)
T	temperature (K)
u	velocity ($m\ s^{-1}$)
W	absorption velocity ($m\ s^{-1}$)
We	Weber number (dimensionless)
w_p	vertical velocity in the pores ($m\ s^{-1}$)

Greek letters

α	thermal conductivity empirical parameter (dimensionless)
B	disjoining pressure parameter (Pa)
β	thermal conductivity empirical parameter (dimensionless)
γ	thermal conductivity empirical parameter (dimensionless)
Λ	dissipation parameter (dimensionless)
μ	viscosity ($kg\ m^{-1}\ s^{-1}$)
ϕ	porosity (dimensionless)
Φ_π	dissipation energy loss rate (W)
Π_c	disjoining pressure (Pa)
ρ	density (kg/m^3)
σ	surface tension (kg/s^{-2})
τ_a	absorption time (s)
θ_e	contact angle (rad)
ξ	boundary immobilisation variable (dimensionless)

Subscripts

∞	ambient air
0	initial value
d	droplet
g	air/gas
l	liquid solvent
max	maximum
p	tablet pores
s	solid
sat	saturated
TD	dried tablet region
v	vapour
WF	wetted tablet region

et al. (2007) reduced the unknown variables in the energy balance equation. They compared their model with others from the literature (Kim and Chun, 2001; Bechtel et al., 1981), achieving better predictions of the maximum spreading factor. The main limitation of their model is its inability to simulate the first milliseconds after impact and predict the droplet rebounding when the equilibrium contact angle has a high value. Recently, Lee et al. (2016) have also used the 1-D model approach to describe the impact of a water droplet on porous stones. Their numerical results were in close agreement with the experimental ones.

In terms of pharmaceutical tablet coating, Shaari (2007) investigated both experimentally and numerically the impact and spreading of a pure liquid water droplet on pharmaceutical tablets. He divided the process into two sub-processes: short-term and long-term. The former involved the first milliseconds after impact when inertial forces are significant and spreading, splashing and rebounding occurs, whereas the latter included penetration and/or wetting. He conducted a series of experiments to investigate the impact behaviour of a droplet on tablet surfaces with different roughness. Using a Volume-Of-Fluid (VOF) CFD model, he described quantitatively the short-term phenomena, but he did not develop any numerical model to describe the long-term phenomena, in particular, absorption.

Bolleddula et al. (2010) studied the impact and spreading behaviour of viscous dispersions and volatile solutions on the surface of a pharmaceutical tablet. They concluded that spreading after impact can be divided into two distinct regimes: the inertia driven regime and the capillarity driven regime. During the inertia driven regime, the diameter reaches an asymptotic value referred to as the maximum spreading factor. Following the inertia driven regime, the droplet continues to spread by capillarity until reaching equilibrium. Their experimental findings with pharmaceutical coatings and tablets will be used in this work for validation.

The capillary spreading of liquids and their absorption into porous substrates is a key process for several applications including pharmaceutical coating. Alleborn and Raszillier (2004) and Siregar et al. (2010) developed mathematical models that describe the absorption of water droplets that are deposited on a permeable solid surface. They solved the Navier–Stokes equation for the spreading of the droplet by employing the lubrication theory approach (Schwartz, 1999) and modelled the liquid movement in the pores using Darcy's equation. The models agreed with experimental results, but their main limitation is that they described spreading and absorption under room ambient conditions that are not generally utilised in pharmaceutical tablet coating processes.

Few researchers have investigated the impact of a droplet on a porous substrate together with the absorption in the medium. Reis et al. (2004) developed a model, based on the finite volume method, that aimed to couple the impact and absorption phenomena of a droplet on a porous medium. They solved the continuity and linear momentum conservation equations to model the fluid flow both outside the porous medium and inside the microscopic pores of the substrate. Their CFD numerical results were in good agreement with experiments they conducted using NMR spectroscopy. Recently, Lee et al. (2016) have coupled their initial semi-empirical model for the first milliseconds after impact with a CFD model for water absorption. They compared their mathematical models with experimental data that they acquired using Neutron Spectroscopy.

Droplet evaporation from within a porous medium is of interest in pharmaceutical coating processes. Understanding the dynamics of the evaporation phenomena can help optimise the water content of the final product. Earlier work (Roberts and Griffiths, 1995; Hu and Larson, 2005; Semenov et al., 2014) was mostly concerned with evaporation of droplets deposited on non-porous surfaces. Roberts and Griffiths (1995) first developed a mathematical model for droplet evaporation from porous surfaces. They validated their numerical results with field and wind tunnel experiments for sand and concrete. Mezhericher et al. (2008) and Golman and Julklang (2013) investigated water evaporation during the slurry droplet drying process. Their modelling approach was adopted in this work in order to develop a novel model that predicts water evaporation from within porous tablets. In our literature search, we were unable to find previous published work that combines the spreading and absorption phenomena of a droplet with evaporation from within a porous medium at high temperature and humidity conditions, conditions that are used in pharmaceutical tablet coating processes.

In this paper, we present a numerical model that describes the spreading, absorption and evaporation of water-based pharmaceutical coating liquids after impingement on porous substrates, e.g. pharmaceutical tablets. Our approach for the initial impact spreading period takes into consideration the high shear viscosities of pharmaceutical coating liquids, enhancing models found in the literature (Bechtel et al., 1981; Roisman et al., 2002; Attane et al., 2007) that only predict the behaviour of low viscosity liquids (water, ethanol). In contrast with previous work (Alleborn and Raszillier, 2004; Siregar et al., 2010), we allowed our (lubrication theory-based) spreading and absorption model to account for the specific operating conditions inside a pharmaceutical pan-coater (high temperature, high air flow, high relative humidity). Our novel evaporation model aims to predict the evaporation-front movement inside the porous medium and to provide information about the water content during the coating process.

We compared our numerical results with experimental data from the literature. Because the validation data for the different parts of our mathematical model were taken from different sources, we validated each part of the overall process (impact-spreading/absorption-evaporation) separately, using the experimental data obtained by different researchers.

2. Mathematical models

In our work, we divided the droplet behaviour into three phases: the kinematic, capillary and evaporation phases. We developed a sub-model for each phase. The first two (Sections 2.1 and 2.2) concern the spreading and absorption of a single droplet, whereas the last one (Section 2.3) simulates the evaporation of the liquid absorbed within the porous matrix of the tablet. Fig. 1 summarises our approach for simulating the overall behaviour of the impinging droplet.

The kinematic phase model describes the first milliseconds after impact during which inertial forces are significant and should not be neglected. Roisman et al. (2002) showed experimentally that the characteristic time of the kinematic phase is of order D_0/U_0, with D_0 and U_0 being the initial diameter of the droplet and the droplet vertical velocity before impact, respectively. We coupled the kinematic phase sub-model with the lubrication theory approach of Alleborn and Raszillier (2004) and Siregar et al. (2010) for the capillary phase, and we additionally accounted for evaporation during absorption. Siregar et al. neglected the evaporation of the droplet during absorption because the evaporation dynamics are significantly slower at the ambient conditions which they studied. However, the temperature, humidity and air flow conditions inside a pharmaceutical pan-coater accelerate evaporation and make its effect not negligible. Finally, we developed a novel sub-model that predicts the evaporation of the liquid absorbed within the porous substrate.

2.1. Kinematic phase

In this section, we present an analytical 1-D spreading model that is based upon the kinetic energy balance equation (Eq. (1)). We made the assumption that during the kinematic phase the absorption phenomena are negligible and the inertial forces are significant. Indeed, in experiments conducted by Shaari (2007), the spreading behaviour of a droplet on a metal (steel) surface was identical to the one on porous tablets for the first milliseconds after impact. Due to the low impact velocity, we also assumed that the coating shape after impact is a spherical cap (Bechtel et al., 1981; Attane et al., 2007). The droplet shapes before and after impingement are shown in Fig. 2.

The motion of the droplet in the first milliseconds after impact is governed by the kinetic energy balance equation (Bechtel et al., 1981):

$$\frac{d(E_k + E_p)}{dt} = -\Phi_\pi \tag{1}$$

where E_k is the kinetic energy, E_p is the potential energy and Φ_π is the kinetic energy loss rate in the droplet due to viscous dissipation.

The assumption for the shape of the droplet to be a spherical cap yielded the following geometric relations between the wetted area radius R_t, droplet maximum height h_{max} and position of the droplet mass center h_m (Attane et al., 2007):

$$R_t^2 = \frac{D_0^2}{3}\left(\frac{D_0}{h_{max}} - \frac{h_{max}^2}{D_0^2}\right); \quad h_m = \frac{1}{6}\left(2h_{max} + \frac{h_{max}^4}{D_0^3}\right) \tag{2}$$

where D_0 is the initial diameter of the spherical droplet before impact. From Eq. (2), one can express the radius and mass center position of the droplet in terms of the maximum droplet height h_{max}. Therefore, we solved the spreading problem (Eq. (1)) for only the variable h_{max} and then calculated the other droplet shape related variables (radius and mass center position) by solving these geometric relations.

The kinetic energy of an incompressible fluid E_k in a volume V is given by the following equation:

$$E_k = \frac{1}{2}\rho \int_v \mathbf{u}\cdot\mathbf{u}\, dV \tag{3}$$

where ρ is the fluid density and $\mathbf{u}$ is the fluid velocity vector.

We described the radial and vertical velocity components inside the droplet, denoted here as u_r and u_z, respectively, by adopting the irrotational flow field first proposed by Bechtel et al. (1981) for impinging droplets:

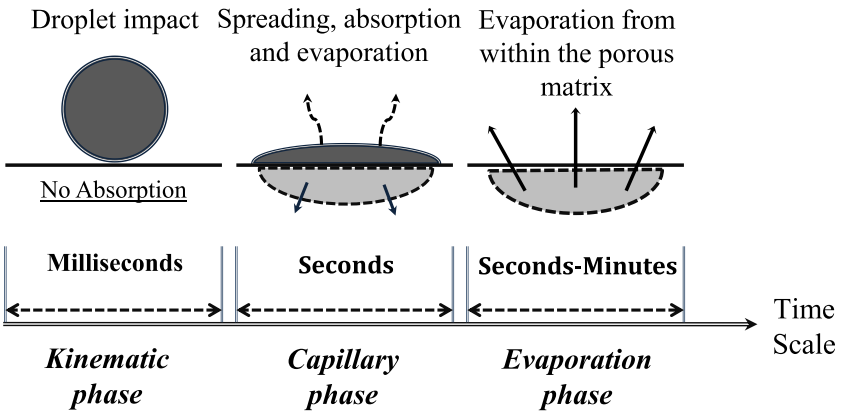

Fig. 1. Mathematical modelling approach.

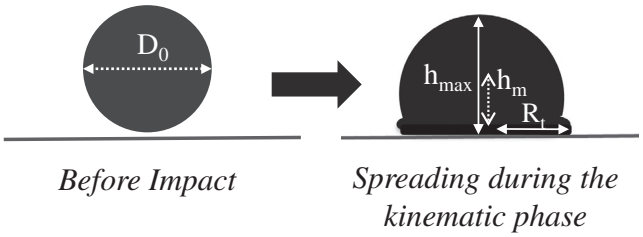

Fig. 2. Droplet spreading during the kinematic phase.

$$u_r = -\frac{1}{2}\frac{1}{h_m}\frac{dh_m}{dt}\,r \tag{4.a}$$

$$u_z = \frac{1}{h_m}\frac{dh_m}{dt}\,z \tag{4.b}$$

Following Bechtel et al. (1981), we integrated Eq. (3) over the volume of a spherical cap of maximum height h_{max} and radius R_t and we obtained:

$$E_k = \frac{1}{2}\,\rho\,\frac{1}{h_m^2}\left(\frac{dh_m}{dt}\right)^2\int_v\left(\frac{r^2}{4}+z^2\right)dV$$
$$= \frac{1}{2}\,\rho\,\pi\,\frac{1}{h_m^2}\left(\frac{R_t^4\,h_{max}}{16}+\frac{13\,R_t^2\,h_{max}^3}{72}+\frac{h_{max}^5}{10}\right)\left(\frac{dh_m}{dt}\right)^2 \tag{5}$$

In Eq. (1), we can express the potential energy term E_p as:

$$E_p = E_g + E_s \tag{6}$$

where E_g is the energy due to the mass of the droplet (gravitational energy) and E_s is the surface energy. The equations we used to calculate E_g and E_s are (Attane et al., 2007):

$$E_g = \frac{\pi}{6}\,\rho\,g\,D_0^3\,h_m \tag{7.a}$$

$$E_s = \sigma\,\pi\left(R_t^2 + h_{max}^2 - R_t^2\,\cos\theta_e\right) \tag{7.b}$$

where σ is the surface tension of the droplet and θ_e is the equilibrium contact angle.

Following de Gennes (1987), we calculated the viscous dissipation energy loss rate as:

$$\Phi_\pi = 2\,\mu\int_v\left[\left(\frac{\partial u_r}{\partial r}\right)^2+\left(\frac{u_r}{r}\right)^2+\left(\frac{\partial u_z}{\partial z}\right)^2\right]dV \tag{8}$$

where μ is the fluid viscosity. Integrating over the volume of the spherical cap we obtained:

$$\Phi_\pi = \frac{\mu\pi}{2}\,\frac{h_{max}}{h_m^2}\left(3\,R_t^2+h_{max}^2\right)\left(\frac{dh_m}{dt}\right)^2 \tag{9}$$

In the literature reviewed, a dissipation parameter is often introduced to fit the experimental data and correct for the model over or under-prediction of the droplet spreading due to the assumed fixed shape. We present in Table 1 the nondimensional dissipation parameter Λ we found in the literature, where Oh denotes the Ohnesorge number ($Oh \equiv \sqrt{We}/Re$, where We is the Weber number and Re is the Reynolds number).

By adding the dissipation parameter, the expression for the viscous dissipation energy loss rate becomes:

$$\Phi_\pi = \frac{\Lambda\,\mu\,\pi}{2}\,\frac{h_{max}}{h_m^2}\left(3\,R_t^2+h_{max}^2\right)\left(\frac{dh_m}{dt}\right)^2 \tag{10}$$

Eq. (10) describes the dissipation energy loss rate for a pure liquid of low viscosity. As mentioned in the introduction section, the mathematical models for the kinematic phase that we found in the literature did not account for polymer solutions with more complex rheology. Bolleddula et al. (2010) measured experimentally the shear viscosity of several coating solutions and investigated the initial spreading after impingement on tablets. By taking into consideration their experimental results, we modified the dissipation parameter and the expression for the modified dissipation parameter Λ' that we propose in this work (to account for the high viscosity of coating liquids) is:

$$\Lambda' = K_\Lambda\sqrt{\pi}\,Oh^{-1/2} \tag{11}$$

where K_Λ is a dimensionless parameter that we introduced to fit the experimental data conducted by Bolleddula et al. (2010) for four liquids of different viscosity: 60% and 85% glycerol/water solutions, Opadry White II 20% and pure water. The liquids chosen for the fitting of the parameter K_Λ cover a wide viscosity range (1–300 cP, Bolleddula et al., 2010). We fitted the parameter K_Λ using gPROMS (Process Systems Enterprise Ltd., 2017), and used regression to derive an equation that expresses K_Λ as a function of the Ohnesorge number (Fig. 3). The equation that calculates K_Λ (with R^2 of 0.95) is:

Table 1
Dissipation parameter Λ from the literature.

Dissipation parameter (Λ)	Literature reference
$\Lambda = \sqrt{\pi}\,Oh^{-1/2}$	Bechtel et al. (1981)
$\Lambda = 10.6\,Oh^{-1/2}$, Low Oh	Kim and Chun (2001)
$\Lambda = 6.4\,Oh^{-1/2}$, High Oh	
$\Lambda = 30\,Oh^{-1/2}$	Attane et al. (2007)

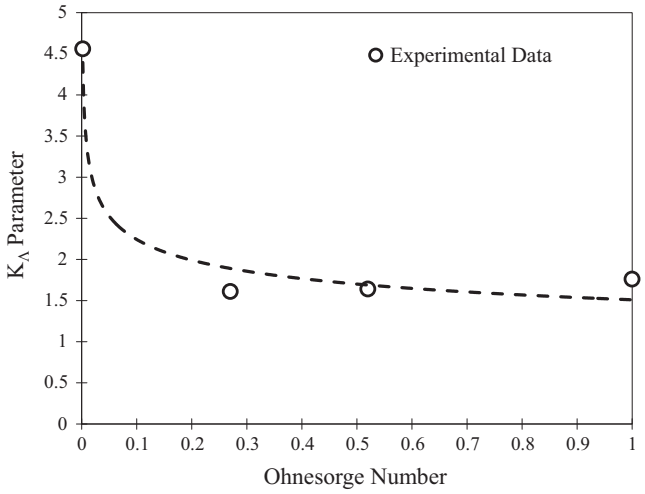

Fig. 3. K_Λ parameter estimation. Experimental data from Bolleddula et al. (2010).

$$K_\Lambda = \frac{3}{2}\, Oh^{-1/6} \tag{12}$$

Therefore, the equation for the revised dissipation parameter becomes:

$$\Lambda' = \frac{3}{2}\,\sqrt{\pi}\, Oh^{-2/3} \tag{13}$$

The revised dissipation parameter was used in our model to predict the behaviour of different Opadry coating droplets that impact on porous tablets with varying impingement velocities, and the performance of this new modified model was compared to work in the literature.

Two initial conditions are required for the solution of the kinematic phase sub-model equations. We considered that the droplet centre of mass (spherical droplet with diameter D_0), just before impact, moves with an impact velocity U_0 directed vertically downward, and that the maximum height of the droplet is equal to the spherical droplet diameter before impingement. These values for the initial conditions (Eqs. (14) and (15)) were taken from the work of Bolleddula et al. (2010).

$$\left.\frac{dh_m}{dt}\right|_{t=0} = -U_0 \tag{14}$$

$$h_{max}|_{t=0} = D_0 \tag{15}$$

The kinematic phase sub-model provides information on the motion of the droplet for the first milliseconds after impact. The rheological properties of the liquid must be known (ρ, σ, μ), together with the initial diameter of the droplet D_0 and the impact velocity U_0, in order to define the parameters of the model. The resulting predictions of the kinematic phase sub-model for the droplet maximum height h_{max}, the droplet mass centre height h_m and wetted area radius R_t were used as an input in the following capillary phase model, which we present next.

2.2. Capillary phase

In the following section, we present the mathematical model that describes the spreading and the absorption of the droplet and the movement of the absorbed liquid in the porous matrix when the capillary effects become dominant. Our model combines the approaches of Alleborn and Raszillier (2004) and Siregar et al. (2010) and additionally accounts for the evaporation of the droplet from the surface during absorption under pharmaceutical coating operating conditions.

2.2.1. Droplet movement on the surface of the porous substrate

The motion of a liquid film or droplet on dry surfaces such as during the capillary driven phase, requires special treatment. This is because the usual "no-slip" boundary condition ($u = 0$) at the solid surface cannot be applied for coatings (lubricant films) that spread on a dry substrate (Szeri, 2010). This is known in the literature (Alleborn and Raszillier, 2004) as the "contact-line singularity problem" and is associated with the fact that there is no solution to the Navier–Stokes equation when we implement the "no-slip" condition on the solid boundary. According to O'Brien and Schwartz (2002), the simplest technique for numerically simulating moving contact lines is to use the notion of a thin precursor film in front of the contact line (whose thickness, h_s, is assumed to be constant). This allows the "no-slip" condition to be applied everywhere.

O'Brien and Schwartz (2002) found that the droplet dynamics are only weakly dependent on the choice of precursor film thickness, and therefore whether such a precursor film layer is real or not is not important. We adopted the precursor film approach and we assumed a precursor film of negligible height ($h_s = 1/100$ of the initial droplet diameter) that spreads across the surface ahead of the wetted area.

The flow of the droplet above the porous layer is governed by the continuity and Navier–Stokes equations:

$$\nabla \cdot \mathbf{u} = 0 \tag{16}$$

$$\rho\left[\frac{\partial \mathbf{u}}{\partial t} + \mathbf{u}\cdot\nabla\mathbf{u}\right] = -\nabla p + \mu\,\nabla^2\mathbf{u} + \rho\,\mathbf{g} \tag{17}$$

where ρ and μ are the density and viscosity of the liquid that forms the droplet, respectively. The fluid is assumed to be incompressible and $\mathbf{u}$ represents the velocity vector.

Solving the full continuity and Navier–Stokes equations is mathematically complex and computationally expensive. A simplification is made possible by the lubrication theory due to the geometry of lubricant films (Szeri, 2010): under normal conditions the in-plane dimension of the film (wetted diameter) is greater than its thickness. The lubrication approximation theory uses scaling to estimate the order of magnitude of the various terms of the continuity and Navier–Stokes equations. The equations are then simplified by deleting those terms that are judged to be too small to have significant effect. Alleborn and Raszillier (2004) and Siregar et al. (2010) both used the lubrication theory approach to solve the Navier–Stokes equations and derived the following equation, written in terms of cylindrical coordinates, that calculates the height profile of the droplet (h):

$$\frac{\partial h(r,t)}{\partial t} = \frac{1}{3\,\mu}\,\frac{1}{r}\,\frac{\partial}{\partial r}\left[r\,h(r,t)^3\,\frac{\partial p(r,t)}{\partial r}\right] - W(r,t) \tag{18}$$

By using the lubrication theory approach formulated in terms of cylindrical coordinates we can accurately describe the behaviour of a spherical cap-shaped coating droplet on a tablet surface (Fig. 4), while simplifying the problem and reducing the computational effort.

In Eq. (18), W is a sink term that accounts for the absorption within the porous substrate. Previous models (Alleborn and Raszillier, 2004; Siregar et al., 2010) assume that evaporation phenomena are negligible during the spreading and absorption of a droplet. That is because the dynamics of evaporation are considerably slower than the dynamics of spreading and absorption. According to experiments performed by Hu and Larson (2005) and Siregar et al. (2010), the characteristic time for the absorption

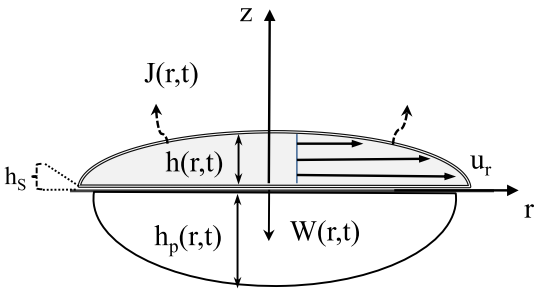

Fig. 4. Droplet spreading, absorption and evaporation.

of a μL droplet is of the order of seconds, while the evaporation of the same droplet, at room temperature, from within a porous medium takes a considerable length of time (100–150 min).

Nonetheless, inside a coating drum the temperature, relative humidity and air flow conditions accelerate evaporation. Therefore, one should not neglect the evaporation of the droplet on the surface of the porous medium during the capillary phase. In our work, we modified Eq. (18) to account for the evaporation velocity (J) during the absorption process:

$$\frac{\partial h(r,t)}{\partial t} = \frac{1}{3\,\mu}\,\frac{1}{r}\,\frac{\partial}{\partial r}\left[r\,h(r,t)^3\,\frac{\partial p(r,t)}{\partial r}\right] - W(r,t) - J(r,t) \tag{19}$$

Eq. (19) predicts the height profile $h(r,t)$ above the surface of a porous tablet in pharmaceutical coating process conditions. To derive an equation for the evaporation velocity J, we assumed a spherical cap droplet shape with a wetted area radius R_t (calculated at the end of the kinematic phase). Following Popov (2005), who investigated the evaporation of sessile droplets, we get:

$$J(r,t) = \frac{\dot{m}_v}{\rho\,\pi\,R_t^2}\left[1 - \left(\frac{r}{R_t}\right)^2\right]^{-1/2} \tag{20}$$

where $\dot{m}_v$ is the vapour mass transfer rate given by the expression (Mezhericher et al., 2008):

$$\dot{m}_v = h_D\left(\rho_{v,d} - \rho_{v,\infty}\right)A_d \tag{21}$$

where h_D is the mass transfer coefficient, A_d is the droplet surface area and $\rho_{v,d}$ and $\rho_{v,\infty}$ are the partial vapour densities over the droplet surface and in the ambient air, respectively.

Following Levi-Hevroni et al. (1995), who investigated the drying of slurry droplets, we estimated the mass transfer coefficient h_D using the Ranz-Marshall correlation for the Sherwood number:

$$Sh \equiv \frac{h_D\,R_t}{\mathcal{D}_v} = 2 + 0.65\cdot Re_d^{1/2}\,Pr_d^{1/3} \tag{22}$$

For a drying process under atmospheric pressure, the diffusion coefficient of water vapour in air, $\mathcal{D}_v$, can be calculated as (Mezhericher et al., 2008):

$$\mathcal{D}_v = 3.564\cdot 10^{-10}\left(T_d + T_g\right)^{1.75} \tag{23}$$

where T_d and T_g are the droplet and air temperatures in Kelvin, respectively. The units for $\mathcal{D}_v$ are m^2/s. In the Ranz-Marshall correlation, Re_d and Pr_d are the Reynolds and Prandtl dimensionless numbers, defined as:

$$Re_d \equiv \frac{R_t\rho_g u_g}{\mu_g};\quad Pr_d \equiv \frac{c_{p,g}\,\mu_g}{k_g} \tag{24}$$

where u_g, μ_g, $c_{p,g}$, ρ_g, k_g are the velocity, viscosity, specific heat, density and thermal conductivity of air, respectively.

To calculate the pressure profile inside the spreading droplet we used the expression of Schwartz et al. (2001) for the motion of liquids onto or from dry substrate areas. Schwartz et al. (2001) took into account the presence of a precursor film and he introduced the "disjoining" pressure Π_c term (which accounts for the van der Walls interactions between the droplet and the solid), writing:

$$p = \rho\,g\,h - \sigma\,\Delta h - \Pi_c;\quad \Delta h \equiv \frac{1}{r}\,\frac{\partial}{\partial r}\left[\frac{r}{\sqrt{1+\left(\frac{\partial h}{\partial r}\right)^2}}\,\frac{\partial h}{\partial r}\right] \tag{25}$$

where Δh is the curvature of the absorbing liquid surface (Siregar et al., 2010) and σ is the liquid surface tension. The relation for the disjoining pressure that Schwartz et al. (2001) used in his work is:

$$\Pi_c = B\left[\left(\frac{h_s}{h}\right)^{n_1} - \left(\frac{h_s}{h}\right)^{n_2}\right] \tag{26}$$

where h_s is the height of the precursor film and B, n_1, n_2 are positive constants with $n_1 > n_2 > 1$. Following Schwartz et al. (2001), we took (n_1, n_2) to be equal to (3, 2) and the constant B to be given by the equation:

$$B = \frac{1}{h_s}\,\frac{(n_1-1)\,(n_2-1)}{2\,(n_1-n_2)}\,\sigma\,\theta_e^2 \tag{27}$$

where θ_e is the equilibrium contact angle of the droplet on the tablet surface.

We considered the absorption velocity (W) to be equal to the vertical velocity, w_p, at the surface of the porous matrix. This velocity will be discussed in the next Section 2.2.2. The equation that calculates W is:

$$W = \begin{cases} w_p\big|_{z=0} & \text{if } h > h_s \\ 0 & \text{if } h < h_s \end{cases} \tag{28}$$

With the above relation we are not allowing the precursor film to be absorbed into the substrate to avoid the contact line singularity issue. The absorption velocity W becomes effectively zero when the droplet height h reaches the characteristic height of the precursor film h_s ($h_s \equiv 1/100\cdot h$, Alleborn and Raszillier, 2004).

2.2.2. Wetting front movement inside the porous medium

For the movement of the wetting front inside the porous matrix and the prediction of the wetting front position, h_p (Fig. 4), we adopted the approach of Siregar et al. (2010), writing:

$$\frac{\partial h_p(r,t)}{\partial t} = -\frac{1}{\phi}\left[\left(u_p(r,z,t)\Big|_{(z=-h_p)}\right)\frac{\partial h_p(r,t)}{\partial r} - \left(w_p(r,z,t)\Big|_{(z=-h_p)}\right)\right] \tag{29}$$

where ϕ denotes the porosity of the porous medium and u_p and w_p are the radial and vertical velocities of the wetting front that are calculated from the Darcy equation:

$$u_p = -\frac{k_p}{\mu}\left(\frac{\partial p_p}{\partial r}\right) \tag{30.a}$$

$$w_p = -\frac{k_p}{\mu}\left(\frac{\partial p_p}{\partial z}\right) \tag{30.b}$$

where p_p is the pressure inside the porous medium and k_p is the permeability of the porous substrate, which we estimated with the Carman-Kozeny equation (Siregar et al., 2010):

$$k_p = \frac{d_p^2\,\phi^3}{180\,(1-\phi)^2} \tag{31}$$

where d_p is the pore diameter. To calculate the pressure of the liquid that is absorbed in the pores, we used the Laplace equation:

$$\nabla^2 p_p = 0 \tag{32}$$

We solved Eqs. (29)–(32) to predict the movement of the wetting front inside the porous matrix.

2.2.3. Boundary conditions

The Eqs. (19)–(32) for the droplet and wetting front movement above and inside the porous substrate are connected by boundary conditions that apply at the surface of the tablet. With Eq. (28) we ensured the mass conservation at the solid–liquid interface by setting the sink term to be equal to the vertical velocity in the pores for $z = 0$. Furthermore, for the pressure continuity across the porous matrix surface, we implemented a dynamic boundary condition at the surface of the tablet:

$$p(r,t) = p_p(r,0,t)\ ,\ \text{for } h > h_s \tag{33.a}$$

$$\left.\frac{\partial p_p(r,z,t)}{\partial z}\right|_{z=0} = 0,\ \text{for } h < h_s \tag{33.b}$$

With Eq. (33.b), we considered that for the dry area ($h < h_s$) the normal derivative of the pressure p_p is zero at $z = 0$. Following the work of Alleborn and Raszillier (2004) and Siregar et al. (2010), we implemented the following conditions at the boundaries of the computational domain (0, R_{max}), where R_{max} is a typical tablet radius that was chosen to be significantly greater than the maximum wetting area radius R_t:

$$\frac{\partial h}{\partial r} = \frac{\partial h_p}{\partial r} = \frac{\partial^3 h}{\partial r^3} = 0, \quad r = 0 \quad \text{and} \quad r = R_{max} \tag{34}$$

These boundary conditions suggest that the slope of the coating droplet surface and the liquid flux vanish across the boundaries of the computational domain. For $r = 0$, Eq. (34) can also be acknowledged as symmetry conditions that are derived from the droplet spherical cap shape assumption. Additionally, as Alleborn and Raszillier (2004), we assumed that the liquid pressure p_p is equal to the capillary pressure at the wetting front:

$$p_p = -\frac{4\,\sigma\,\cos\theta_e}{d_p}, \quad z = -h_p(r,t) \tag{35}$$

The above condition is applied at a boundary that changes with time (z = wetting front depth = $-h_p$). The way we manipulated the moving boundary problem is presented in the numerical solution Section 2.2.4.

2.2.4. Numerical solution

We made dimensionless the equations that describe the capillary phase using the following dimensionless variables:

$$r^* \equiv \frac{r}{R_0},\ h^* \equiv \frac{h}{H_0},\ z^* \equiv \frac{z}{H_0},$$

$$h_p^* \equiv \frac{h_p}{H_0},\ t^* \equiv \frac{\sigma H_0^3}{\mu R_0^4}\,t,\ p^* \equiv \frac{H_0}{\sigma}\,p,$$

$$p_p^* \equiv \frac{H_0}{\sigma}\,p_p,\ w_p^* \equiv \frac{\mu}{\sigma}\,w_p,\ u_p^* \equiv \frac{\mu}{\sigma}\,u_p,$$

$$W^* \equiv \frac{\mu R_0^4}{\sigma H_0^4}\,W,\ \Pi_c^* \equiv \frac{H_0}{\sigma}\,\Pi_c,\ R_t^* \equiv \frac{R_t}{R_0}$$

where R_0 is a characteristic droplet radius and H_0 is a characteristic droplet height. In our work, we defined R_0 and H_0 to be the wetted area radius (R_t) and the maximum droplet height (h_{max}) after the completion of the kinematic phase, respectively.

For the behaviour of the liquid above the surface i.e. for $0 < r^* < R_t^*$, after substituting the dimensionless variables in Eqs. (19), (20) and (25) we obtained:

$$\frac{\partial h^*}{\partial t^*} = \frac{R_0^2}{3\,H_0^2}\,\frac{1}{r^*}\,\frac{\partial}{\partial r^*}\left(r^*\,h^{*3}\,\frac{\partial p^*}{\partial r^*}\right) - W^* - J^* \tag{36.a}$$

$$J^* = \frac{\mu\,R_0^2}{\pi\,\rho\,\sigma\,H_0^4}\,\dot{m}_v\left(1 - r^{*2}\right)^{-1/2} \tag{36.b}$$

$$p^* = \frac{\rho\,g\,H_0^2}{\sigma}\,h^* - \frac{H_0^2}{R_0^2}\,\Delta h^* - \Pi_c^* \tag{36.c}$$

Eq. (36.a) calculates the droplet height profile h(r,t), while Eqs. (36.b) and (36.c) provide information on the evaporation rate of the droplet and the pressure inside the liquid, respectively. The Eqs. (29), (30.a), (30.b), (32) that describe the movement of the liquid inside the porous medium (for $0 < r^* < R_t^*$ and $-h_p^* < z^* < 0$) become in dimensionless form:

$$\frac{\partial h_p^*}{\partial t^*} = -\frac{R_0^4}{H_0^4\,\phi}\left[\frac{H_0}{R_0}\,u_p^*\Big|_{(z^*=-h_p^*)}\,\frac{\partial h_p^*}{\partial r^*} - w_p^*\Big|_{(z^*=-h_p^*)}\right] \tag{37.a}$$

$$w_p^* = -\frac{k_p}{H_0^2}\left(\frac{\partial p_p^*}{\partial z^*}\right) \tag{37.b}$$

$$u_p^* = -\frac{k_p}{H_0\,R_0}\left(\frac{\partial p_p^*}{\partial r^*}\right) \tag{37.c}$$

$$\frac{H_0^2}{R_0^2}\,\frac{1}{r^*}\,\frac{\partial}{\partial r^*}\left(r^*\,\frac{\partial p_p^*}{\partial r^*}\right) + \frac{\partial^2 p_p^*}{\partial z^{*2}} = 0 \tag{37.d}$$

Eq. (37.a) predicts the wetting front (water penetration depth measured from the surface of the substrate) while Eqs. (37.b)–(37.d) calculate the velocity and pressure profile of the fluid that is absorbed into the porous medium. Our model consists of equations that are defined in a moving domain (Eqs. (37.b)–(37.d)). The wetting front depth changes with time and therefore every variable defined between 0 and $h_p(r,t)$ has no fixed boundaries.

Since the moving boundaries are a function of time and their location needs to be determined to derive the solution, our mathematical model is non-linear. In general, the non-linearity associated with the moving boundary usually makes the analysis of this class of problems challenging. The most common example of this category of problems is the mathematical model of the melting of ice that was first developed by Stefan (Kutluay et al., 1997).

It is possible to fix the moving boundaries of a problem by using a fixed coordinate system in space for the moving boundary condition. The transformation proposed by Landau (1950) is:

$$\xi \equiv \frac{z^*}{h_p^*(r^*,t^*)} \tag{38}$$

With the help of this transformation, the moving interface $z^* = -h_p^*(r^*,t^*)$ is fixed at $\xi = -1$. We implemented the above transformation to our partial differential equations (Eqs. (37.b)–(37.d)) that are defined in the z-direction between 0 and $h_p^*(r,^*t^*)$:

$$w_p^* = -\frac{k_p}{H_0^2\,h_p^{*2}}\left(\frac{\partial p_p^*}{\partial \xi}\right) \tag{39.a}$$

$$u_p^* = -\frac{k_p}{H_0\,R_0}\left(-\frac{\xi}{h_p^*}\,\frac{\partial h_p^*}{\partial r^*}\,\frac{\partial p_p^*}{\partial \xi} + \left.\frac{\partial p_p^*}{\partial r^*}\right|_{\xi}\right) \tag{39.b}$$

$$\frac{1}{r^*}\frac{\partial}{\partial r^*}\left(-\frac{\xi\, r^*}{h_p^*}\frac{\partial h_p^*}{\partial r^*}\frac{\partial p_p^*}{\partial \xi}+\left.\frac{\partial p_p^*}{\partial r^*}\right|_{\xi}\right)\Bigg|_{\xi} - \frac{1}{r^*}\frac{\xi}{h_p^*}\frac{\partial h_p^*}{\partial r^*}\frac{\partial}{\partial \xi}\left(-\frac{\xi\, r^*}{h_p^*}\frac{\partial h_p^*}{\partial r^*}\frac{\partial p_p^*}{\partial \xi}+\left.\frac{\partial p_p^*}{\partial r^*}\right|_{\xi}\right) + \left(\frac{R_0}{H_0}\right)^2\frac{1}{h_p^{*2}}\frac{\partial^2 p_p^*}{\partial \xi^2}=0 \tag{39.c}$$

Using Landau's transformation, we modified our model equations so that the new boundaries change in the vertical direction (inside the porous medium) from $-h_p^*(r^*,t^*) < z^* < 0$ to $-1 < \xi < 0$.

Eqs. (36.a)–(37.a) and (39.a)–(39.c) constitute the mathematical model for the capillary phase that we propose to couple with the kinematic phase sub-model presented earlier to predict the behaviour of a pharmaceutical coating droplet after impingement on a porous surface. The inputs we defined were the wetted area radius R_t and the maximum height of the droplet h_{max}, which where calculated from the kinematic phase model (Section 2.1). As an output, we derived the droplet height profile h, the wetting front depth h_p and the absorption time τ_a. We used the evaporation phase sub-model predictions for the height profile h of the droplet and the wetting front depth h_p as inputs for the evaporation model, which we present next.

2.3. Evaporation phase

In this section, we describe the novel mathematical model that we developed to predict the evaporation from within a porous substrate where the liquid is depleted from the tablet surface. With this model we aimed to analyse the effect of air and droplet temperatures on the drying of the pharmaceutical tablet. The effect of the tablet porosity was also studied. As mentioned in the introduction, we adopted a model for the drying of slurry droplets. The crust formed on the surface of the droplet represents the dried tablet, whereas the wet core represents the still wetted part of the tablet (Fig. 5).

2.3.1. Mathematical model

We calculated the temperature profile in the tablet using the following equations of energy conservation (Golman and Julklang, 2013):

$$\left[\phi\,\rho_l\,c_{p,l}+(1-\phi)\,\rho_s\,c_{p,s}\right]\frac{\partial T_{WF}}{\partial t}=k_{WF}\,\frac{\partial^2 T_{WF}}{\partial z^2},\quad -h_{ep,max}\leqslant z\leqslant -H_p(t) \tag{40.a}$$

$$\left[\phi\,\rho_g\,c_{p,g}+(1-\phi)\,\rho_s\,c_{p,s}\right]\frac{\partial T_{TD}}{\partial t}=k_{TD}\,\frac{\partial^2 T_{TD}}{\partial z^2},\quad -H_p(t)< z\leqslant 0 \tag{40.b}$$

where T_{TD} and T_{WF} are the temperatures in the dry and wetted parts of the tablet, respectively. Eq. (40.a) holds for the wetted region (Fig. 5) which lies between the evaporation front depth H_p and maximum wetted depth $h_{ep,max}$, whereas Eq. (40.b) holds for the dry crust region that is located between the porous matrix surface and the evaporation front depth. The parameters $c_{p,s}$, $c_{p,l}$, $c_{p,g}$ and k_{WF} and k_{TD} are the heat capacities of the solid, liquid and gas phases, respectively, and the conductivities of the wetted and dry regions of the porous matrix, respectively.

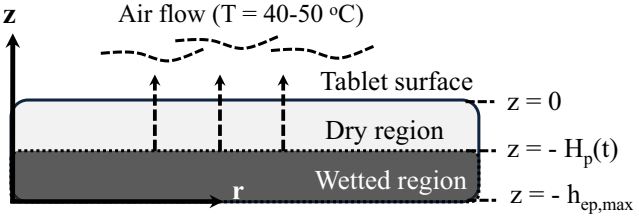

Fig. 5. Liquid evaporation from within the porous substrate.

We estimated the thermal conductivities of the dry and wetted sections of the tablet using the Woodside and Messmer model (Woodside and Messmer, 1961). They combined empirical equations for series and parallel distributions of solid, liquid and vapour phases in a porous medium:

$$k_{TD}=\frac{\alpha\,k_s\,k_v}{k_s\,(1-\beta)+\beta\,k_v}+\gamma\,k_v \tag{41.a}$$

$$k_{WF}=\frac{\alpha\,k_s\,k_l}{k_s\,(1-\beta)+\beta\,k_l}+\gamma\,k_l \tag{41.b}$$

where k_s is the thermal conductivity of the porous substrate, and k_v and k_l are the thermal conductivities of the vapour and liquid solvent (water), respectively. The parameters α, β and γ are estimated using the following equations: $\alpha = 1-\gamma, \beta = (1-\phi)/\alpha$, and $\gamma = \phi - 0.03$, respectively (Woodside and Messmer, 1961).

To solve the energy conservation equations (Eqs. (40.a) and (40.b)), we used the following boundary conditions:

$$\frac{\partial T_{WF}}{\partial z}=0,\quad z=-h_{ep,max} \tag{42.a}$$

$$T_{WF}=T_{TD},\quad z=-H_p(t) \tag{42.b}$$

$$\phi\,\rho_l\,h_{fg}\frac{dH_p}{dt}=k_{TD}\,\frac{\partial T_{TD}}{\partial z}-k_{WF}\,\frac{\partial T_{WF}}{\partial z},\quad z=-H_p(t) \tag{42.c}$$

$$h_{heat}\,(T_g-T_{TD})=k_{TD}\,\frac{\partial T_{TD}}{\partial z},\quad z=0 \tag{42.d}$$

where h_{fg} is the evaporation latent heat and h_{heat} is the heat transfer coefficients. In Eq. (42.a), we set the temperature T_{WF} gradient in the z-direction at the wetting front boundary ($z=-h_{ep,max}$) equal to zero. This is a symmetry condition justified by the fact that the line z = - $h_{ep,max}$ is regarded as a symmetry line between the part of the tablet shown in Fig. 5 and the specular part not reported. The boundary condition (42.b) states that the dry and wetted section temperatures are equal at the evaporation front ($z=-H_p$). Finally, Eqs. (42.c) and (42.d) represent the enthalpy jump conditions (Delhaye, 1974) at the wetting front and at the tablet surface, respectively.

The vapour concentration in the dry region is obtained from the mass balance:

$$\phi\frac{\partial C_v}{\partial t}=\mathcal{D}_{TD}\frac{\partial^2 C_v}{\partial z^2} \tag{43}$$

where $\mathcal{D}_{TD}$ is the effective vapour diffusivity.

We formulated Eq. (43) assuming that the accumulation of vapour in the pores balances the transfer of water vapour to the particle surface by a diffusive mechanism. We estimated the effective vapour diffusivity in the porous medium ($\mathcal{D}_{TD}$) using the empirical equation found in Golman and Julklang (2013):

$$\mathcal{D}_{TD}=\mathcal{D}_{WF}\,\phi^{1.9} \tag{44.a}$$

$$\mathcal{D}_{WF}=0.22\cdot 10^{-4}\left(\frac{T_g}{273.15}\right)^{1.75} \tag{44.b}$$

where T_g is the air temperature in Kelvin. The units of $\mathcal{D}_{WF}$ are m^2/s.

We can write the Neumann boundary conditions for the mass balance equation (Eq. (43)) as (Golman and Julklang, 2013):

$$-\mathcal{D}_{TD}\frac{\partial C_v}{\partial z} = h_D\left(C_{v_{z=0}} - C_{v_g}\right), \quad z = 0 \tag{45.a}$$

$$\phi\,\rho_l\frac{dH_p}{dt} = -\mathcal{D}_{TD}\,M_{w,l}\,\frac{\partial C_v}{\partial z}, \quad z = -H_p(t) \tag{45.b}$$

where C_v is the vapour concentration and $M_{w,l}$ is the molecular weight of the liquid that evaporates.

Following Golman and Julklang (2013), we calculated the vapour concentration in the air bulk C_{vg} from the equation:

$$C_{vg} = \frac{RH\,\rho_{v,sat}}{M_{w,l}} \tag{46}$$

where $\rho_{v,sat}$ is the saturated vapour density in the air and RH is the relative humidity.

We evaluated the mass (h_D) and heat (h_{heat}) transfer coefficients from the Ranz-Marshall correlations for the Nusselt (Nu) and Sherwood (Sh) numbers (Mezhericher et al., 2008):

$$Nu \equiv \frac{h_{heat}\,S_{ep}}{k_g} = 2 + 0.65\cdot Re^{1/2}Pr^{1/3} \tag{47.a}$$

$$Sh \equiv \frac{h_D\,S_{ep}}{\mathcal{D}_{WF}} = 2 + 0.65\cdot Re^{1/2}Sc^{1/3} \tag{47.b}$$

where S_{ep} denotes the diameter of the circular evaporation interface of the absorbed droplet as seen in Fig. 6. In Eqs. (47.a) and (47.b), Re, Pr, Sc are the Reynolds, Prandtl and Schmidt numbers, respectively. These are given by the following equations:

$$Re \equiv \frac{u_g\,\rho_g\,S_{ep}}{\mu_g}, \quad Pr \equiv \frac{c_{p_g}\,\mu_g}{k_g}, \quad Sc \equiv \frac{\mu_g}{\rho_g\,\mathcal{D}_{WF}} \tag{48}$$

where u_g, μ_g, c_{p_g}, ρ_g are the velocity, viscosity, specific heat and density of the air, respectively.

As seen in Fig. 6, the initial condition for the wetting front profile in the evaporation phase can be provided by the capillary phase sub-model (Section 2.2). The wetted area inside the porous tablet can be estimated from the evaporation depth H_p (Fig. 6). This will be discussed in Section 3.3.

2.3.2. Numerical solution

To numerically solve Eqs. (40.a)–(47.b), we first made them dimensionless and then applied Landau's boundary immobilisation technique (Kutluay et al., 1997) for the equations that involve the moving evaporation front. We made the equations dimensionless using the following variables:

$$r^* \equiv \frac{r}{R_t},\; z^* \equiv \frac{z}{h_{ep,max}},\; H_p^* \equiv \frac{H_p}{h_{ep,max}},$$

$$t^* \equiv t\,\frac{\mathcal{D}}{h_{ep,max}},\; T^* \equiv T\,\frac{c_{p,s}}{h_{fg}},\; C_v^* \equiv C_v\,\frac{M_{w,l}}{\rho_l}$$

To perform the Landau's transformation we divided the z^* domain into two sub-domains z_1^* and z_2^* as seen in Fig. 7. The transformed variables are:

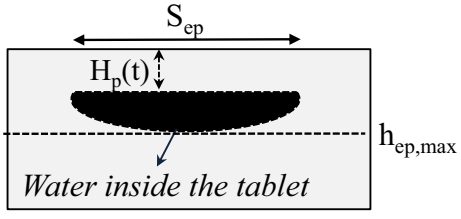

Fig. 6. Prediction of the final evaporation front H_p.

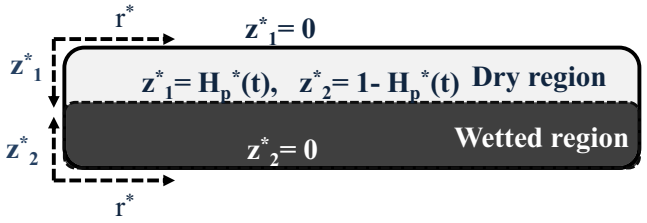

Fig. 7. Domains z_1^* and z_2^*.

$$\xi \equiv \frac{z_1^*}{H_p^*(t^*)}, \quad \xi' \equiv \frac{z_2^*}{H_{p,l}^*(t^*)} \tag{49}$$

Here $H_{p,l} = h_{ep,max} - H_p$. Landau's transformation, modified our model equations so that the new boundaries change in the vertical direction (inside the porous medium) from $0 < (z_1^*, z_2^*) < (H_p^*, H_{p,l}^*)$ to $0 < (\xi, \xi') < 1$.

The dimensionless equations for the temperature profile are:

$$\left[\phi\,M_{EB,1l} + (1-\phi)M_{EB,1s}\right]\left(\frac{\partial T_{WF}^*}{\partial t^*} + \frac{\xi}{1-H_p^*}\frac{dH_p^*}{dt^*}\frac{\partial T_{WF}^*}{\partial \xi}\right) = \frac{1}{(1-H_p^*)^2}\frac{\partial^2 T_{WF}^*}{\partial \xi^2}, \quad 0 \leqslant \xi \leqslant 1 \tag{50.a}$$

$$\left[\phi\,M_{EB,2g} + (1-\phi)M_{EB,2s}\right]\left(\frac{\partial T_{TD}^*}{\partial t^*} - \frac{\xi'}{H_p^*}\frac{dH_p^*}{dt^*}\frac{\partial T_{TD}^*}{\partial \xi'}\right) = \frac{1}{H_p^{*2}}\frac{\partial^2 T_{TD}^*}{\partial \xi'^2}, \quad 0 \leqslant \xi' \leqslant 1 \tag{50.b}$$

For the concentration profile we get:

$$\phi\left(\frac{\partial C_v^*}{\partial t^*} - \frac{\xi'}{H_p^*}\frac{dH_p^*}{dt^*}\frac{\partial C_v^*}{\partial \xi'}\right) = \frac{1}{H_p^{*2}}\frac{\partial^2 C_v^*}{\partial \xi'^2}, \quad 0 \leqslant \xi' \leqslant 1 \tag{51}$$

where

$$M_{EB,1l} \equiv \frac{\rho_l\,c_{p,l}\,\mathcal{D}_{WF}}{k_{WF}}, \quad M_{EB,1s} \equiv \frac{\rho_s\,c_{p,s}\,\mathcal{D}_{WF}}{k_{WF}},$$
$$M_{EB,2g} \equiv \frac{\rho_g\,c_{p,g}\,\mathcal{D}_{TD}}{k_{TD}}, \quad M_{EB,2s} \equiv \frac{\rho_s\,c_{p,s}\,\mathcal{D}_{TD}}{k_{TD}}$$

The boundary conditions (Eqs. (42.a)–(42.d) and (45.a), (45b)) become in dimensionless form:

$$\frac{\partial T_{WF}^*}{\partial \xi} = 0, \quad \xi = 0 \tag{52.a}$$

$$T_{WF}^* = T_{TD}^*, \quad \xi = \xi' = 1 \tag{52.b}$$

$$\left(T_g^* - T_{TD}^*\right) = M_{TD}\frac{1}{H_p^*}\frac{\partial T_{TD}^*}{\partial \xi'}, \quad \xi' = 0 \tag{52.c}$$

$$M_{b,TD}\frac{1}{H_p^*}\frac{\partial T_{TD}^*}{\partial \xi'} - M_{b,WF}\frac{1}{1-H_p^*}\frac{\partial T_{WF}^*}{\partial \xi} = \phi\,\frac{dH_p^*}{dt^*}, \quad \xi = \xi' = 1 \tag{52.d}$$

$$M_{mb}\left(C_{v_{z=0}}^* - C_{v_g}^*\right) = \frac{1}{H_p^*}\frac{\partial C_v^*}{\partial \xi'}, \quad \xi = 0 \tag{52.e}$$

$$\frac{dH_p^*}{dt^*} = -\frac{1}{H_p^*}\frac{\partial C_v^*}{\partial z^*}, \quad \xi' = 1 \tag{52.f}$$

where

$$M_{TD} \equiv \frac{k_{TD}}{h_{ep,max}\, h_{heat}}, \quad M_{mb} \equiv \frac{h_{ep,max}\, h_D}{\mathcal{D}_{TD}},$$

$$M_{b,TD} \equiv \frac{k_{TD}}{\rho_l\, cp_s\, \mathcal{D}_{TD}}, \quad M_{b,WF} \equiv \frac{k_{WF}}{\rho_l\, cp_s\, \mathcal{D}_{WF}}$$

By solving Eqs. (50.a)–(52.f), we were able to simulate water evaporation from within a porous substrate of uniform porosity. The part of the mathematical model presented above is a novel approach, based on the drying of slurry droplets, that aims to calculate the water content evaporation from within a porous tablet. This model can be used to simulate tablet drying inside a coating drum and to thereby predict the water content in the final product. The validation of the model we developed in this work is presented in the following section.

3. Results and discussion

We validated the numerical results from the model described above with experiments from the literature. Because the experimental data were taken from multiple sources, we did not investigate a single case study, instead we compared our model predictions with independent experimental studies of different researchers. In the following sections, we analyse and validate the numerical results for the kinematic, capillary and evaporation (from within the porous matrix) phases, respectively. All the numerical calculations were performed in gPROMS (Process Systems Enterprise Ltd., 2017), employing the Modelbuilder modelling platform.

Some of the input parameters of our models were difficult to determine precisely from the experimental results from the literature. To account for this, we propagated the experimental measurement errors of the input parameters to the numerical results of the model following the stochastic sampling method of Cacuci and Cacuci (2003). First, we defined the probability distributions (measurement error) of the input parameters based on experimental data we found in the literature. Subsequently, we used these distributions to generate a sample and create multiple scenarios for each sub-model presented in Section 2. Lastly, we performed a series of simulations and we calculated the standard deviation of the response variables (Cacuci and Cacuci, 2003). The propagated errors of the numerical results, we calculated using the method of Cacuci and Cacuci, appear as error bars in the figures of this section.

3.1. Kinematic phase numerical results

In the following section, we present the numerical results of the kinematic phase sub-model (Section 2.1) along with the propagated measurement errors of the input parameters and we compare these with experimental data from Bolleddula et al. (2010) and Lee et al. (2016).

3.1.1. Case study 1

Bolleddula et al. (2010) investigated the spreading of viscous pharmaceutical coatings (Table 2) that contained different percentage of solids, while Lee et al. (2016) considered pure water droplets. The experimental measurement errors of the liquid coating properties (density, surface tension and shear viscosity) were assumed to be ±5% (Bolleddula et al., 2010). The values of the nondimensional parameter K_Λ that appear in Table 2 were estimated for different Ohnesorge numbers by solving Eq. (13). Note that the model presented in this work is predictive and not fitted. Therefore, the numerical results for the liquids Opadry White II 20%, 60% and 80% glycerol/water solutions, are not presented here as they were used for the fitting of the parameter K_Λ and are considered biased.

Fig. 8(a) shows the numerical prediction for the diameter of the wetted area together with experimental results of Bolleddula et al. (2010) for the coating liquid Opadry White II 10 %. The droplet diameter before impact was taken to be 2.5 mm (as in the validation experiments taken from Bolleddula et al., 2010) and we investigated three impact velocity scenarios: 0.41 m/s, 0.93 m/s and 2.47 m/s. In Fig. 8, the dashed error lines for the numerical results are the propagated measurement errors of the model input parameters (liquid coating properties), whereas for the validation data, the error bars stand for the droplet height measurement error that was estimated based on the graphs presented by Bolleddula et al. (2010).

The numerical solutions closely predict the spreading behaviour of the coating droplet for all impact velocities considered. The results illustrate that the kinematic phase takes place in the characteristic time U_0/D_0 (Roisman et al., 2002), where U_0 is the impact velocity and D_0 is the diameter of the droplet before impact on the tablet. After that characteristic time (1 ms, 2 ms and 5 ms, respectively, for the three impact velocities examined), the spreading affected by inertial forces seems to be negligible as the wetted area diameter and spreading factor reach a plateau.

Bolleddula et al. (2010) presented most of their experimental results in terms of a spreading factor. The spreading factor is the ratio of the diameter of the wetted area to the initial diameter of the droplet. In Fig. 8(b), we compare the numerical results for the spreading factor of different coating droplets ($D_0 = 2.5$ mm) that are deposited on tablet surfaces with the experimental data available (Bolleddula et al., 2010). The numerical results are in good agreement with the experimental data for all three coating liquids (Opadry White II 10%, 12%, 15%).

The ability of our kinematic phase model to predict the droplet maximum height h_{max} during the first milliseconds of spreading is illustrated in Fig. 9. The model calculates the maximum height of an Opadry White II 10% coating droplet and closely predicts the behaviour reported from the experiments of Bolleddula et al. (2010). The ability of the numerical model to predict both the maximum height of the droplet and the wetted area diameter for low impact velocities (Fig. 8) shows that the assumption we made in this work for the shape of the droplet (spherical cap shape) is valid for impact velocities less than 2.5 m/s. These low spray impact velocities (0.41–2.5 m/s) are often utilised in pharmaceutical coating processes to avoid splashing phenomena that can affect inter-tablet coating uniformity (Amidon et al., 1999).

In Table 3, we present the simulation results for an Opadry White II 10% droplet, with initial diameter 2.5 mm and impingement velocity 2.47 m/s, together with the corresponding experimental values from Bolleddula et al., 2010. The error for the numerical results (±0.02 mm) represents the propagated measurement errors of the model input parameters (liquid coating proper-

Table 2
Coating droplets rheology properties. Experiments from Bolleddula et al. (2010).

Coating	Density (kg/m^3)	Surface tension (N/m)	Viscosity (mPa s) @1000 s^{-1}	K_Λ
Opadry White II 10%	1020	0.04822	98	1.61
Opadry White II 12%	1030	0.04766	175	1.64
Opadry White II 15%	1040	0.04667	377	1.70

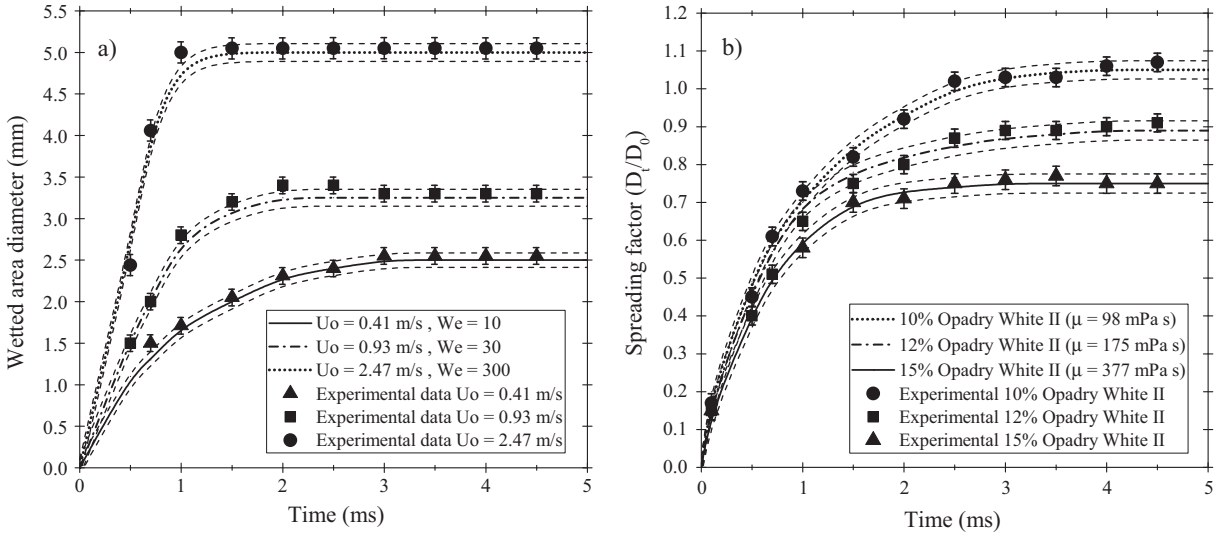

Fig. 8. Validation with experimental data from Bolleddula et al. (2010): (a) Wetted area diameter of 10% Opadry White II coating droplets ($D_0 = 2.5$ mm) for different impact velocities. (b) Spreading factor of droplets of different viscosity after deposition.

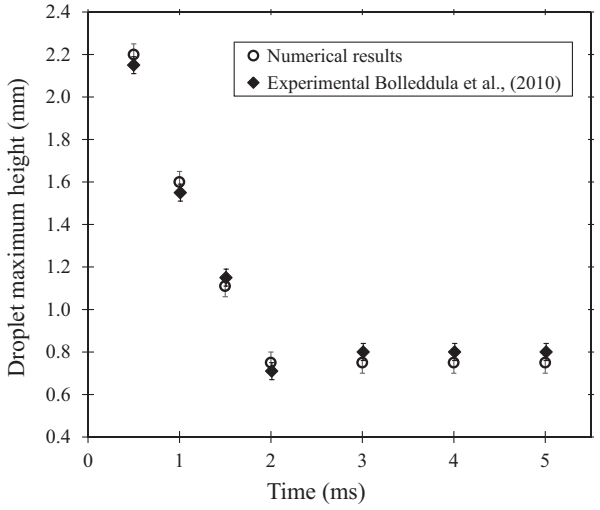

Fig. 9. Maximum coating height during the spreading of an Opadry White II 10% droplet. Initial droplet diameter = 2.5 mm, Impact velocity $U_0 = 2.47$ m/s. Validation with experiments from Bolleddula et al. (2010).

Table 3
Validation of the maximum droplet height (h_{max}) with experiments from Bolleddula et al. (2010) for the kinematic phase.

Time (ms)	Maximum droplet height (mm)		% |Error|
	Numerical results	Experiments	
0.0	2.50	2.50	0.0%
0.5	2.20	2.15	2.3%
1.0	1.59	1.55	2.6%
2.0	1.11	1.15	3.5%
3.0	0.73	0.70	4.3%
4.0	0.75	0.80	6.3%
5.0	0.75	0.80	6.3%

ties, impact velocity and initial droplet diameter). Comparing the mean values of the numerical model predictions and experimental data illustrates a small percentage error (<6.2%).

Bolleddula et al. (2010) mentioned in their conclusions that the model from the literature which better predicted their experimental data for large droplets was the one from Roisman et al. (2002). We compared the numerical results of our kinematic phase sub-model and of the model of Roisman et al. (2002) with the experimental data for the three Opadry White II coatings (impact velocity = 0.93 m/s) obtained by Bolleddula et al. (2010). The percentage errors of the spreading factor at the end of the inertia driven regime for both models are reported in Table 4. This shows that the model presented in this work predicts the behaviour of the coating droplets (investigated by Bolleddula et al., 2010) better than the model from Roisman et al. (2002).

3.1.2. Case study 2

Lee et al. (2016) investigated the spreading of pure water droplets on porous substrates. We used their experimental results to validate our model for water droplets. Different numerical results were calculated employing different dissipation parameters Λ (Table 1) found in the literature for pure liquids. Fig. 10 compares the experimental data for the diameter of the wetted area with the model predictions (derived using different Λ). The spherical water droplet in the experiment and the numerical simulations had an initial diameter of 2 mm and an impact velocity of 1 m/s. The initial wetted area diameter was taken to be 0, as the surface was assumed completely dry before the impingement of the droplet. The numerical results that we calculated employing the Λ parameter of Bechtel et al. (1981) are in good agreement with the experimental data. Bechtel et al. (1981) worked only with spherical cap droplets, in contrast with the other authors referenced in Table 1, who investigated several shapes and impact velocities. The spherical cap shape is encountered when the impact velocity is low. Therefore, since in our work we investigated slow impingement velocities, one may expect that the dissipation parameter of Bechtel is the most appropriate for water droplet spreading during the kinematic phase.

The comparison among the dissipation parameters found in the literature shows that the kinematic phase sub-model (Section 2.1) is able to estimate the spreading of pure liquid droplets when we apply the appropriate dissipation parameter Λ. The numerical results that were calculated using the dissipation parameter of Bechtel et al. (1981) shown in Fig. 10 are also presented in Table 5 to better illustrate the ability of the model to predict the spreading of pure water droplets. We also included the percentage error absolute values of the wetted area diameter that are shown in the last column of Table 5.

Table 4
Comparison of the current model with the mathematical model from Roisman et al. (2002) in terms of the final spreading factor during the kinematic phase. Experiments from Bolleddula et al. (2010).

Coating liquid	Final Spreading Factor		Experiments (Bolleddula et al.)	% |Error|	
	This work	Roisman et al.		This work	Roisman et al.
Opadry White II 10%	1.31	1.42	1.30	0.1%	9.2%
Opadry White II 12%	1.23	1.33	1.20	2.5%	10.8%
Opadry White II 15%	1.03	1.17	1.00	3.0%	17.0%

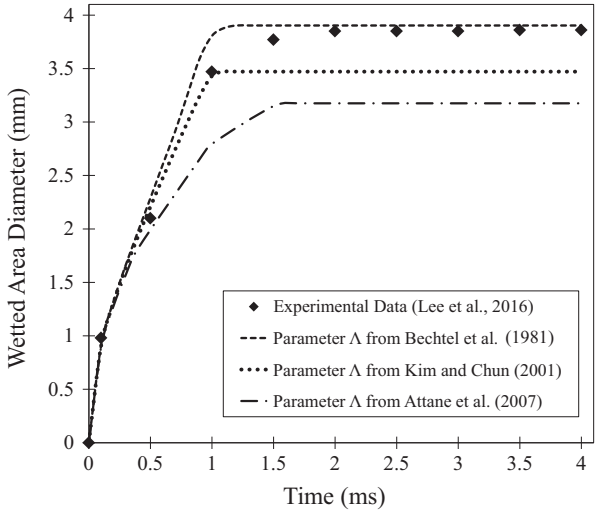

Fig. 10. Wetted area diameter after impact of a 2 μL water droplet $U_0 = 1$ m/s. Comparison between different dissipation parameters from the literature and experimental data from Lee et al. (2016).

Table 5
Validation of the numerical results for the wetted area diameter during the kinematic phase with experiments from Lee et al. (2016). Numerical results acquired using the dissipation parameter $\Lambda = \sqrt{\pi}Oh^{1/2}$ from Bechtel et al. (1981). Propagated numerical model error = ±0.10 mm; experimental data measurement error = ±0.05 mm.

Time (ms)	Wetted area diameter (mm)		% |Error|
	Numerical results	Experimental data	
0.0	0.00	0.00	0.0%
0.1	0.92	0.95	3.2%
0.5	2.29	2.30	0.1%
1.0	3.61	3.45	4.6%
2.0	3.90	3.85	1.3%
4.0	3.90	3.80	2.6%

In Table 5, the error for the response (wetted area diameter, ±0.10 mm) represents the propagated measurement errors of the model input parameters we took from the work of Lee et al. (2016), whereas for the validation data, the error (±0.05 mm) stands for the droplet height measurement error that was estimated based on the graphs presented by Lee et al. (2016). The small absolute percentage error (<5%) of the model results highlights the model capability to simulate efficiently the spreading of pure liquids droplet when the appropriate dissipation parameter is introduced.

The numerical results presented in Section 3.1.1 (Case study 1) are in good agreement with the experimental data obtained from several water-based pharmaceutical coating droplets. The model also provides good estimates for the spreading of pure water droplets (Case study 2). Overall, coating droplets tend to spread less than pure water droplets owing to their higher viscosity. The numerically calculated wetted area diameters and maximum droplet heights for different impact scenarios (impingement velocity, initial droplet diameter) and different liquids are all in good agreement with the experimental measurements of Bolleddula et al. (2010) and Lee et al. (2016).

3.2. Capillary phase numerical results

In this section, we present the results for the capillary phase model and we compare them with experimental data from the literature. The initial time ($t = 0$) for the numerical results of the capillary phase model is taken to be the time when the inertial forces become negligible at the end of the kinematic phase. The experimental data were taken from the recent paper of Lee et al. (2016). They used high-speed imaging and neutron radiography to quantify water absorption in porous materials (porous stones) from droplet deposition until depletion. For the validation of our capillary phase model we assumed that the behaviour of the absorbed droplet does not change significantly if the substrate is a pharmaceutical tablet of similar porosity and pore diameter.

In Fig. 11, we compare the capillary phase model predictions and experimental data regarding the percentage of water content that is absorbed inside porous substrates (Savonniéres and Meule stones) after impact of a 4.3 mg droplet on their surface. The numerical results and experimental data regarding the Savonniéres and Meule stones are presented in Fig. 11 with circles and diamonds, respectively. The small overprediction during the first seconds is probably due to the inability of the current model to account for the effect of the air trapped between the droplet and the substrate. The trapped air can impede the absorption of the droplet (Lee et al., 2016). The results of the mathematical model presented in this work follow the trend of the neutron radiography experimental data by Lee et al. (2016) with a mean percentage error of 5.1%.

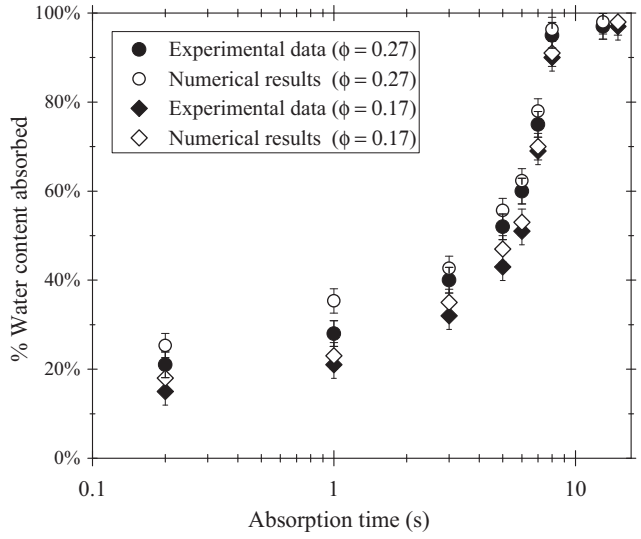

Fig. 11. Percentage of liquid content that is absorbed inside the porous substrate for Savonnieres ($\phi = 0.27$) and Meule ($\phi = 0.17$) stones. Experimental data from Lee et al. (2016).

The ability of the model to predict the depth of the maximum wetting front distance from the surface ($h_{p,max}$) is illustrated in Table 6 which compares with experimental data for Meule stones (porosity = 16.6 ± 0.3% and pore diameter = 9.1 ± 1.5 μm, viscosity = 1 cP, surface tension = 72 mN·m^{-1}). The measurement errors for the input parameters (porosity, pore diameter) were found in the paper of Lee et al. (2016). This initial uncertainty for the porous matrix properties was propagated using the stochastic sampling method (Cacuci and Cacuci, 2003). The model predictions, along with their propagated error, are compared with experimental data whose error bars were estimated from the graphs presented by Lee et al. (2016).

Our mathematical model for the capillary phase allows the dynamic simulation of spreading and absorbing water droplets. Fig. 12(a) and (b) illustrate the numerical results for the liquid movement above and below the porous substrate (Savonniéres stone) surface, respectively. The porous matrix ($\phi = 26.9 \pm 1.4\%$, $d_p = 10.3 \pm 3.5$ μm) was assumed completely dry before the deposition of the droplet (droplet volume = 4.3 μL). Fig. 12(a) and (b) show the depletion of the liquid from the surface and the evolution of the wetting front in the porous matrix. The dotted lines in Fig. 12 represent the propagated measurement errors of the model input parameters. The absorption time calculated by the model (12 s) is the same as the one reported in the work of Lee et al. (2016).

Fig. 13(a) and (b) compare capillary phase model results with experimental data for water droplet absorption in Savonniéres porous stones (Lee et al., 2016). The error bars for the numerical results are estimated by propagating the uncertainty for the porosity and pore diameter of the Savonniéres stones. Both the numerical results for the maximum droplet height (Fig. 13(a)) and the distance of the wetting front the surface of the porous substrate (Fig. 13(b)) are in good agreement with the experimental data of Lee et al. (2016).

Overall, the ability of the model to predict the height of the water droplet above the substrate and the depth of the liquid (wetting) front inside the porous matrix can be used to predict the water content on the surface and inside a pharmaceutical tablet during the film coating process. The chemical affinity of the solvent (water) and the pharmaceutical tablet needs to be investigated as part of future work, since the assumption made at the beginning of this section that the behaviour of the absorbed liquid is not affected by the choice of porous material does not hold in the case of highly hydrophilic or hydrophobic substrates.

3.2.1. Evaporation during the capillary phase

Previous models assume that the evaporation phenomena are negligible during the spreading and absorption of a droplet (Alleborn and Raszillier, 2004; Siregar et al., 2010). This is because only the liquid absorption at room temperature and humidity conditions was considered. However, inside a coating drum, the temperature, relative humidity and air flow conditions accelerate evaporation. Therefore, in our work we took into account the evaporation velocity (Eq. (20)) that affects the amount of liquid that is absorbed into the porous substrate. Fig. 14(a) and (b) illustrate the difference in the absorption process between a model that neglects evaporation and our approach. For our approach, we chose operating conditions that resemble those inside a pharmaceutical pan-coater ($T_g = 50$ °C, relative humidity = 50%), whereas for the model that neglects evaporation we did not account for the evaporation term on the right-hand side of Eq. (19).

The numerical results show that the effect of evaporation during the capillary phase is significant when the ambient conditions are similar to those in a pharmaceutical pan-coater. The droplet height profile in Fig. 14(a) is significantly lower ($\simeq 0.5$ mm), after 3 s of absorption, when we account for the evaporation from the surface. Similarly, the final wetting front depth (distance from the surface) in Fig. 14(b) is higher when we include the evaporation from the surface velocity in our calculations.

The present model takes into account the evaporation from the substrate surface during absorption and thus enables a more accurate prediction of the absorbing liquid behaviour in coating operating conditions. The current approach allows the consideration of elevated temperature, humidity level and ambient air flow and provides results that more accurately describe the water droplet behaviour in a pharmaceutical pan-coater.

Table 6
Comparison between the numerical results and experimental data for the maximum wetting front depth during the capillary phase. Experiments from Lee et al. (2016). Propagated numerical model error = ±0.06 mm; experimental data measurement error = ±0.05 mm.

Time (s)	Maximum wetting front depth (mm)		% |Error|
	Numerical results	Experimental data	
0	0.00	0.00	0.0%
3	−1.03	−1.00	3.0%
6	−1.52	−1.50	1.3%
9	−1.70	−1.65	3.0%
12	−1.78	−1.70	4.7%

3.3. Evaporation phase numerical results

In this section, we present the numerical results of the evaporation model. The evaporation model was presented in Section 2.3 and describes the rate of liquid depletion from within the porous matrix. For validation, we compared the numerical results with experimental data taken from the work of Reis et al. (2003) and Tag et al. (2013). Reis et al. performed their experiments with glass beads, while Tag et al. worked with pharmaceutical tablets. All the experimental data reported in this work were derived from experiments conducted at room ambient temperature. The present model, however, can be applied for other coating process operating conditions as well, as previously discussed.

Fig. 15(a) compares the numerical results with the experimental water evaporation from within a $CaCO^3$ tablet (Tag et al., 2013) at conditions of low temperature ($T_g \simeq 20$ °C) and high relative humidity (RH = 50%). The $CaCO^3$ tablets of the experiments had a porosity (ϕ) of 0.08 and the wetted region (shaped like a spherical cap, Fig. 2) had a maximum wetted front depth ($h_{ep,max}$) of 1.2 mm. The liquid evaporation from within the porous matrix is quite slow due to the relatively low ambient temperature, high relative humidity, small porosity and the lack of air flow on the surface of the tablet. The numerical results from the solution of the model proposed in this work are in good agreement with the experimental data as the mean relative error is 0.76%.

In Fig. 15(b), we validate the evaporation model with experimental data for glass beads. The experiments were conducted by Reis et al. (2003) at room ambient conditions with no air flow over the porous matrix (stagnant air). The glass beads had a size of 50 μm and the overall porous matrix had a porosity ϕ of 0.42. The evaporation rate in the experiments conducted by Reis et al. (2003) is higher than the one observed by Tag et al. (2013). This is due to the higher porosity of the glass beads that allows the evaporating water vapour to diffuse easier through the pores. The numerical results are very close to the corresponding experimental data with a mean relative error of 2%.

The error bars of the numerical results presented in Fig. 15(a) and (b) were estimated in this work by propagating the experimental measurement errors for the porosity and pore diameter which are assumed to be the same as in the capillary phase (taken

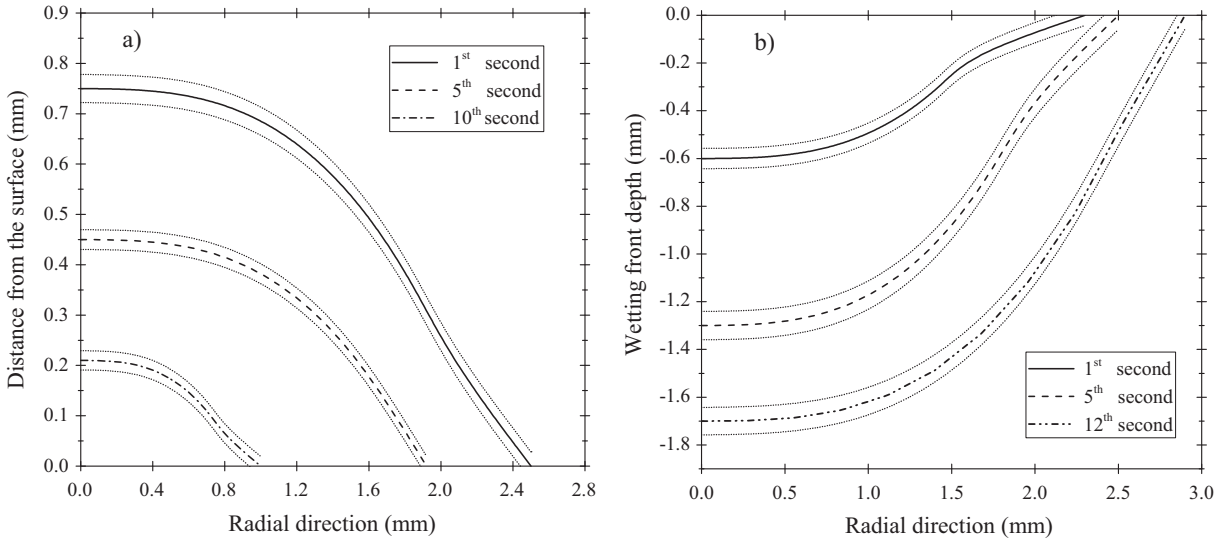

Fig. 12. (a) Droplet height profile on the surface after 1, 5 and 10 s and (b) wetting front profile in the substrate after 1, 5 and 12 s.

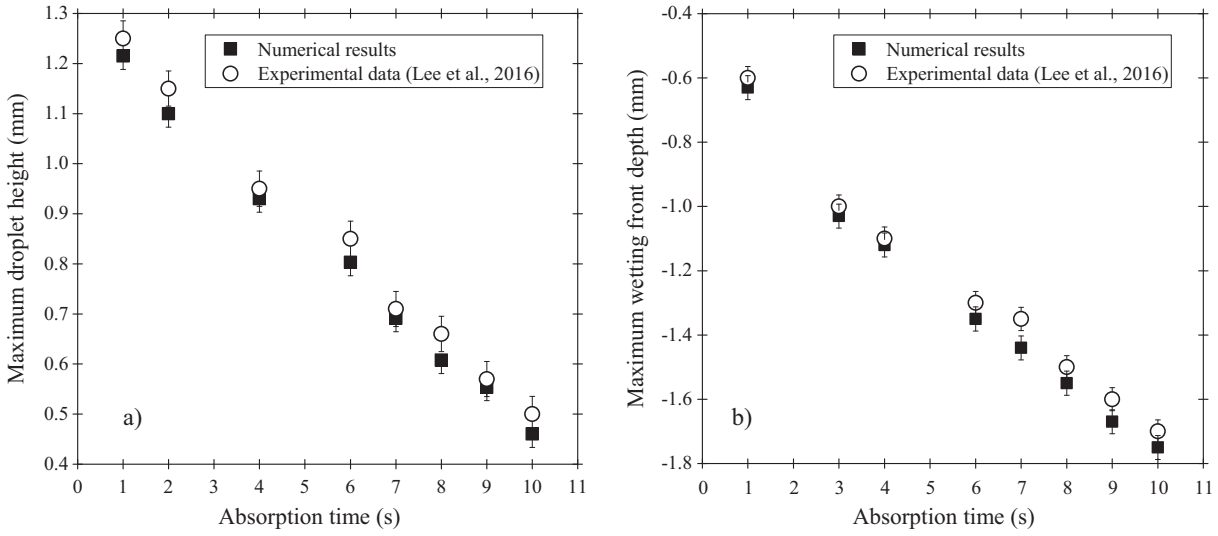

Fig. 13. Comparison between simulation and experimental data for (a) the maximum droplet height on the substrate surface and (b) the maximum wetting depth in the substrate. Experimental data from Lee et al. (2016).

from Lee et al., 2016). Tag et al. (2013)also mentioned a deviation in the room temperature (20–27 °C) which was taken into account in our calculations. The experimental data errors were estimated from the figures presented in the paper of Tag et al. (2013) and Reis et al. (2003).

We can calculate the wetted region profile (Fig. 5) inside the porous matrix during the final evaporation phase by subtracting the advancing evaporation front depth H_p (Fig. 6) from the wetting front depth h_p, calculated at the end of the capillary phase (Section 2.2). We performed simulations for the glass beads used in the experiments of Reis et al. (2003). Fig. 16 presents the numerical results for the wetted region profile inside the porous matrix after 60 and 120 min, respectively. In Fig. 16, the origin of the z-coordinate represents the evaporation front depth H_p calculated by Eqs. (52.d) and (52.f).

The results appearing in Fig. 16 resemble the experimental data of Reis et al. (2003). However, the prediction error of the wetted region profile during the evaporation phase can be high considering the lack of information for the water permeability of the porous materials investigated by Reis et al. (2003). In addition, the error of the experimental measurements reported by Reis et al. (2003) was high as well.

In Fig. 17, even though we are unaware of any experimental data for validation, we present the model prediction for the wetted region position inside a porous substrate during the evaporation phase. For the numerical simulation, we chose operating conditions that resemble those inside a pan-coater during the pharmaceutical film coating process ($T_g = 50$ °C, $RH = 70\%$, $u_g = 1$ m/s). The initial volume of water in the pores was 4 μL. In Fig. 17, the origin of the z-coordinate represents the evaporation front depth H_p. The mathematical model presented in this work suggests that the complete evaporation of a 4 μL water droplet absorbed into a porous tablet ($\phi = 0.20$) takes 6 min.

The validation of the numerical results with the experimental data from the two separate papers shows that our novel evaporation mathematical model is able to efficiently predict the water content evaporation from different materials in different conditions. The experimental results of both Reis et al. (2003) and Tag et al. (2013), which are successfully estimated by the current evaporation model, show that the depletion of water from within a por-

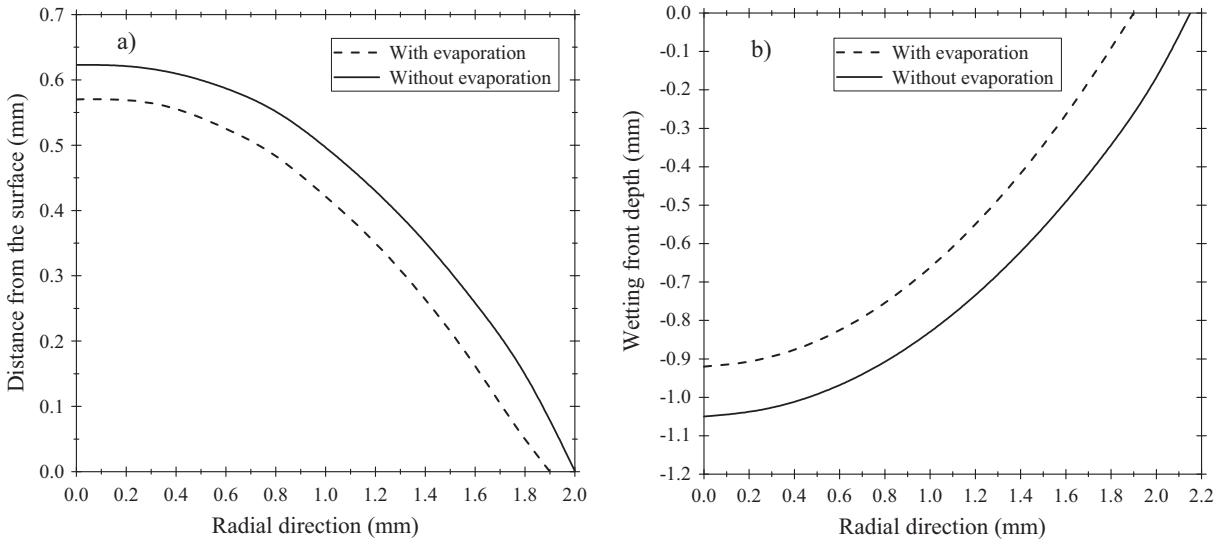

Fig. 14. Effect of evaporation in liquid absorption during the capillary phase, (a) Droplet height profiles after 3 s. (b) Final wetting front profile inside the porous matrix.

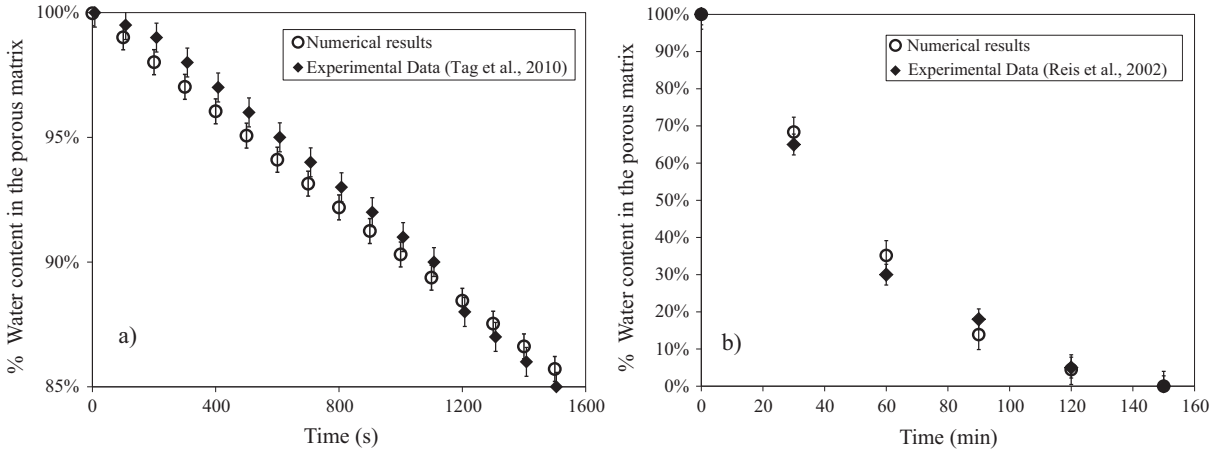

Fig. 15. Evaporation of water content inside (a) $CaCO_3$ tablets ($\phi = 0.08$) and (b) glass beads ($\phi = 0.42$) during the evaporation phase. Experiments from (a) Tag et al. (2013) and (b) Reis et al. (2003).

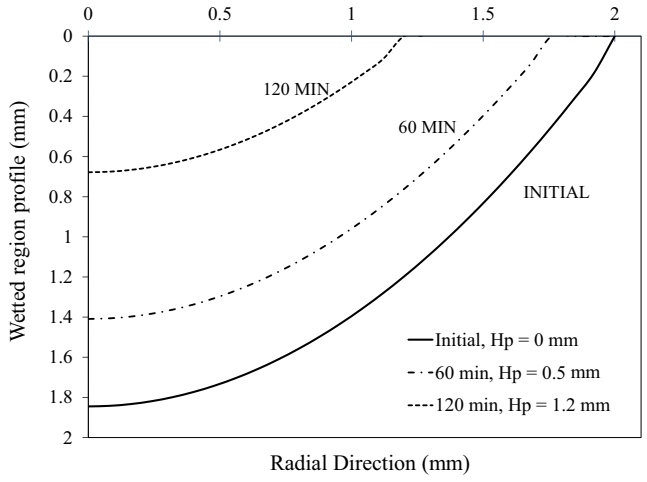

Fig. 16. Wetted region profile in glass beads. (Substrate porosity = 0.42. Initial water volume = 4 μL).

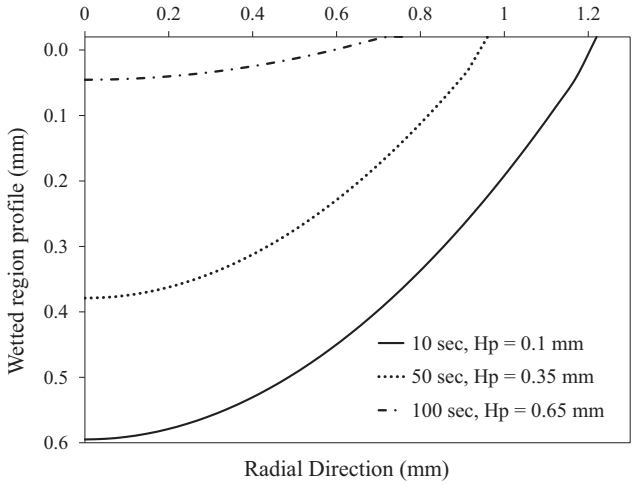

Fig. 17. Wetting front depth profile during the evaporation phase under coating process conditions. (Substrate porosity = 0.20. Initial water volume = 4 μL).

ous matrix can take a significant amount of time. Pharmaceutical tablets in coating process operating conditions will dry notably faster due to higher temperatures and air flow. The numerical results for the water content inside the porous matrix, and the distance of the wetted front from the surface, can be used to predict the final water content inside a pharmaceutical tablet during the coating process.

4. Conclusions

The mathematical model presented in this paper aimed to numerically simulate the behaviour of an aqueous polymer solution droplet after impingement on a porous tablet in pharmaceutical coating process conditions. We combined successfully the 1-D droplet spreading model for the initial impact period with the lubrication theory approach for the receding and absorption of the coating liquid and then simulated the evaporation from within the porous medium with a separate model. The combination of the three sub-models that we presented in this paper is a novel approach that can provide an estimate for the water content of a pharmaceutical tablet after droplet impingement during coating.

The validation with experimental data from different studies showed that our numerical model is predictive and can be used to simulate droplet impact, spreading, absorption and evaporation from porous pharmaceutical tablets. The 1-D energy equation model that we adopted accurately simulated the spreading of the droplet during the first milliseconds after impact when the inertial forces are significant. Moreover, the capillary phase model based on the lubrication theory approach of Alleborn and Raszillier (2004) and Siregar et al. (2010)was successfully coupled with the initial impact model and enhanced to include a prediction for evaporation during absorption. The spreading and absorption numerical results were validated with experimental data from Bolleddula et al. (2010) and Lee et al. (2016). Finally, the model we developed for the evaporation phase from inside the porous medium accurately predicted experimental data taken from different studies (Reis et al., 2003; Tag et al., 2013).

Our work aims to provide information about the aqueous colloidal suspension coating process that is widely utilized within the pharmaceutical industry. Therefore, the modification of the existent sub-models proposed here is useful in order to be able to simulate the spreading and absorption of coating films on tablet surfaces. Furthermore, the droplet size we investigated in this work was significantly larger that the one utilised in pharmaceutical tablet coating processes. However, further experiments are needed to test if our model is predictive for micrometer droplets. Finally, the lack of information regarding the properties of the substances used by the pharmaceutical industry poses a problem; experiments should be performed to provide insight into the interactions between the porous tablet materials and the solvents used in the film coating process.

Acknowledgements

The authors wish to acknowledge the financial support given to this research project by the Engineering Physical Science Research Council (EPSRC), grant code EP/M507581/1, and Eli Lilly and Company.

References

Alleborn, N., Raszillier, H., 2004. Spreading and sorption of a droplet on a porous substrate. Chem. Eng. Sci. 59 (10), 2071–2088.
Amidon, G.L., Lee, P.I., Topp, E.M. (Eds.), 1999. Transport Processes in Pharmaceutical Systems. CRC Press.
Attane, P., Girard, F., Morin, V., 2007. An energy balance approach of the dynamics of drop impact on a solid surface. Phys. Fluids 19 (1).
Bechtel, S.E., Bogy, D.B., Talke, F.E., 1981. Impact of a liquid drop against a flat surface. IBM J. Res. Dev. 25 (6), 963–971.
Bolleddula, D.A., Berchielli, A., Aliseda, A., 2010. Impact of a heterogeneous liquid droplet on a dry surface: application to the pharmaceutical industry. Adv. Colloid Interface Sci. 159 (2), 144–159.
Cacuci, D.G., Cacuci, C.G., 2003. Sensitivity and Uncertainty Analysis. Chapman & Hall/CRC Press, Boca Raton.
de Gennes, P.G., 1987. Polymers at an interface: a simplified view. Adv. Colloid Interface Sci. 27 (3–4), 189–209.
Delhaye, J.M., 1974. Jump conditions and entropy sources in two-phase systems. Local instant formulation. Int. J. Multiph. Flow 1 (3), 395–409.
Golman, B., Julklang, W., 2013. Analysis of drying kinetics of a slurry droplet in the falling rate period of spray drying. Int. J. Chem. Mol. Nucl. Mater. Metall. Eng. 7 (9), 685–689.
Hu, H., Larson, R.G., 2005. Analysis of the microfluid flow in an evaporating sessile droplet. Langmuir 21 (9), 3963–3971.
Kim, H., Chun, J., 2001. The recoiling of liquid droplets upon collision with solid surfaces. Phys. Fluids 13 (3), 643–659.
Kutluay, S., Bahadir, A.R., Ozdes, A., 1997. The numerical solution of one-phase classical Stefan problem. J. Comput. Appl. Math. 81 (1), 135–144.
Landau, H.G., 1950. Heat conduction in a melting solid. Quarterly of Applied Mathematics 8 (1), 81–94.
Lee, J.B., Radu, A.I., Vontobel, P., Derome, D., Carmeliet, J., e et al., 2. Absorption of impinging water droplet in porous stones. J. Colloid Interface Sci. 471, 59–70.
Levi-Hevroni, D., Levy, A., Borde, I., 1995. Mathematical modelling of drying of liquid/solid slurries in steady state one-dimensional flow. Drying Technol. 13 (5–7), 1187–1201.
Mezhericher, M., Levy, A., Borde, I., 2008. Modelling of particle breakage during drying. Chem. Eng. Process. 47 (8), 1404–1411.
O'Brien, S.B.G., Schwartz, L.W., 2002. Theory and modeling of thin film flows. Encycl. Surface Colloid Sci., 5283–5297
Park, H., Carr, W.W., Zhu, J., Morris, J.F., 2003. Single drop impaction on a solid surface. AIChE J. 49 (10), 2461–2471.
Popov, Y.O., 2005. Evaporative deposition patterns: spatial dimensions of the deposit. Phys. Rev. E 71 (3), 036313.
Process Systems Enterprise Ltd., 2017. gPROMS User Guide.Release 4.2.0. London, UK. <www.psenterprise.com/gproms>.
Reis, N.C., Griffiths, R.F., Mantle, M.D., Gladden, L.F., 2003. Investigation of the evaporation of embedded liquid droplets from porous surfaces using magnetic resonance imaging. Int. J. Heat Mass Transf. 46 (7), 1279–1292.
Roberts, I.D., Griffiths, R.F., 1995. A model for the evaporation of droplets from sand. Atmos. Environ. 29 (11), 1307–1317.
Roisman, I.V., Rioboo, R., Tropea, C., 2002. Normal impact of a liquid drop on a dry surface: model for spreading and receding. Proc. Roy. Soc. A: Math. Phys. Eng. Sci. 458, 1411–1430.
Schwartz, L.W., Roy, R.V., Eley, R.R., Petrash, S., 2001. Dewetting patterns in a drying liquid film. J. Colloid Interface Sci. 234 (2), 363–374.
Schwartz, L.W., 1999. Theoretical and numerical modeling of coating flow on simple and complex substrates including rheology, drying and Marangoni effects. Advances in coating and drying of thin films, 105–128.
Semenov, S., Trybala, A., Rubio, R.G., Kovalchuk, N., Starov, V., Velarde, M.G., 2014. Simultaneous spreading and evaporation: recent developments. Adv. Colloid Interface Sci. 206, 382–398.
Shaari, K.Z.K. 2007. Coating Uniformity on a Pharmaceutical Tablet: An Experimental Study and Finite Volume Modeling of Droplet Impact Behavior (PhD thesis). Morgantown, West Virginia, United States.
Siregar, D.P., Kuerten, J.G.M., Wijshoff, H.M.A., Van der Linden, L.T.M., 2010. Numerical simulation of the absorption of a droplet in a porous medium. In: Vafai, K. (Ed.), AIP Conference Proceedings, vol. 1254, No. 1, pp. 135-140.
Szeri, A.Z., 2010. Fluid Film Lubrication. Cambridge University Press, Cambridge.
Tag, C.-M., Toiviainen, M., Ridgway, C., Juuti, M., Gane, P.A.C., 2013. Dynamic ink oil absorption in a pigmented porous coating medium studied by near-infrared diffuse reflectance spectroscopy. Transp. Porous Media 99 (1), 145–160.
Woodside, W., Messmer, J.H., 1961. Thermal conductivity of porous media. I. Unconsolidated sands. J. Appl. Phys. 32 (9), 1688–1699.